IEEE Access
Multidisciplinary | Rapid Review | Open Access Journal

Received January 10, 2019, accepted January 22, 2019, date of publication February 1, 2019, date of current version February 20, 2019.

Digital Object Identifier 10.1109/ACCESS.2019.2897013

Comprehensive Development and Control of a Path-Trackable Mecanum-Wheeled Robot

JOE SIANG KEEK, SER LEE LOH, AND SHIN HORNG CHONG, (Senior Member, IEEE)
Center of Robotics and Industrial Automation, Faculty of Electrical Engineering, Universiti Teknikal Malaysia Melaka, Durian Tunggal 76100, Malaysia
Corresponding author: Ser Lee Loh (slloh@utem.edu.my)

This work was supported in part by the Skim Zamalah UTeM Scholarship, and in part by the High Impact PJP Grant of Universiti Teknikal Malaysia Melaka under Grant PJP/2017/FKE/HI11/S01536.

ABSTRACT This paper presents an intuitively straightforward yet comprehensive approach in developing and controlling a Mecanum-wheeled robot (MWR), with decent path tracking performance by using a simple controller as an end objective. The development starts by implementing two computer ball mice as sensors to realize a simple localization that is immune toward wheel slippage. Then, a linearization method by using open-loop step responses is carried out to linearize the actuations of the robot. Open-loop step response is handy, as it directly portrays the non-linearity of the system, thus achieving effective counteraction. Then, instead of creating a lookup table, polynomial regression is used to generate an equation in which the equation later represents an element of the linearizer. Next, a linear angle-to-gain (LA-G) method is introduced for path tracking control. The method is as easy as just linearly maps the summation of two angles—the angle between immediate and desired positions and the MWR's heading angle, into gains to control the wheels. Unlike the conventional control method which involves inverse kinematics, the LA-G method is directly a displacement-controlled approach and does not require the knowledge of parametric values, such as the robot's dimensions and wheel radius. Finally, all the methods are implemented, and the MWR experimentally demonstrates successfully tracking various paths, by merely using proportional controllers.

INDEX TERMS Localization, linearization, Mecanum wheel, motion control, path tracking.

I. INTRODUCTION

Ever since the invention of Mecanum wheel by Bengt Ilon in 1970s, the characteristic of the wheel has been studied thoroughly by many researchers. At early stage, the advantage of being maneuverable has drawn much attention of researchers and engineers and immediately they deploy the advantage into daily lives; for industrial application i.e. automated guided vehicle (AGV) [1] and mobile robot manipulator [2], and for non-industrial application i.e. wheelchair [3]. Today, the application of Mecanum wheel for industry as robot manipulator [4] and AGV [5] remain and are improved, whereas non-industrial application has expanded to mobile humanoid manipulator for kitchen [6] and even robotic waiter for restaurant [7]. The influence of Mecanum wheel for the past decades is evident and today, many sectors are still celebrating the benefits brought by the technology.

However, apart from its diversification in application, the remaining of the studies are mostly on counteracting uncertainties caused by the wheel, such as low and varying wheel-floor friction, shifting of wheel-floor contact point, irregular wheel radius, vibrating movement and so on [8]–[10]. Since these drawbacks represent the natures of Mecanum wheel, therefore they cannot be removed totally, but instead, can be reduced or overcame through hardware design i.e. implementing suspension system [6], [11] or improved sensory system i.e. on-board vision sensor [1], [4], [12], off-board vision sensor [13], [14], ultrasonic sensor [3], [15], inertial measurement unit (IMU) [16]–[18], and so on. With improved computational power and wireless communication, positioning by using wireless signal and machine vision is considered as the summit of current localization technology [19]. The controller implemented for Mecanum-wheeled robot (MWR) to attain autonomous path tracking and control has also evolved as well since the past decades; from proportional-integral-derivative (PID) controller [1]–[3] to fuzzy logic controller (FLC) [20]–[22], and then adaptive controller [23], [24]. FLC relies on the knowledge and experience of human to design rules and functions, whereas adaptive control requires the knowledge of dynamic models.

The associate editor coordinating the review of this manuscript and approving it for publication was Ali Zemouche.

2169-3536 © 2019 IEEE. Translations and content mining are permitted for academic research only.
Personal use is also permitted, but republication/redistribution requires IEEE permission.
See http://www.ieee.org/publications_standards/publications/rights/index.html for more information.

Although the proposed advanced control methods do display promising result, but the process of modeling the controller requires more efforts when compared with PID controller.

Most of the control method proposed for MWR has inverse kinematics equation at the bottom of the MWR control system's hierarchy. Modeling of the equation requires not only the knowledge and accuracy of known physical parameters, but is derived in a condition where uncertainty and modeling error are assumed to be non-existing [25], [26]. Robust adaptive control may then required to be located at the upper layer of the control hierarchy, where modeling of uncertainties is performed [23]. As modeling of closed-loop control system for MWR is complicated, manual remote control based on common standards and patterns as shown in Figure 1 is sometimes preferred for both competition and industrial application. This is quite unfortunate because the advantages of being flexible and maneuverable are not fully utilized up to what the wheel is capable of.

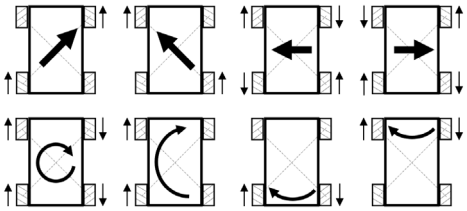

FIGURE 1. Standard operation pattern as reference for control of Mecanum-wheeled robot (MWR).

Instead of sophisticated modeling and controller design, this paper presents a comprehension on developing and controlling an MWR in tracking complex paths, with only simple proportional (P) controller. This paper is organized as follows. Section II starts with positioning system (localization) for our MWR. Section III discusses non-linearity of the MWR and linearization of the actuators. Then, Section IV introduces linear angle-to-gain (LA-G) method, which is an intuitive path tracking control method that enables the MWR to maneuver on any desired path. Section V examines, validates and discusses path-tracking performance of the MWR through experiments and finally, Section VI concludes this paper.

II. LOCALIZATION

The most conventional dead-reckoned positioning method for wheeled mobile robot is by using motor-coupled encoder. However, things are a bit different when it comes to Mecanum-wheeled robot (MWR). Mecanum wheel has smaller contact area (point of contact) compared with conventional wheel (line of contact) with floor, and is thus prone to slippage [27]. Also, Mecanum wheel has inconsistent radius due to compression of roller, and varying wheel-floor contact point during motion (see [8], [9]. These uncertainties imply that localization by using motor-coupled encoder for MWR is infeasible. A non-motor-coupled sensor for dead-reckoned positioning is preferable. Therefore, in this paper, computer ball mouse is selected as positioning sensor and slippage on the Mecanum wheel no longer affects the positioning of our MWR. The MWR is equipped with two computer ball mice so that three degree-of-freedom (3 DOF) of localization can be achieved. Localization by using computer mouse can be seen in [28] and [29] as well, but the mouse used in the literatures is optical typed. Optical mouse has drawback in which its sensitivity changes according to the characteristic of the floor surface [29], [30]. This, however, does not happen to computer ball mouse and therefore is selected for our MWR. Figure 2 illustrates the MWR in global coordinate frame.

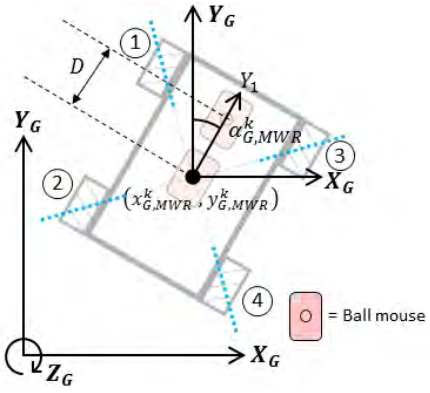

FIGURE 2. Layout of the MWR in global coordinate system.

Blue dotted line are axes of the rollers that are contacting with the floor. Notations X_G, Y_G and Z_G are axes of the global coordinate frame whereas X_m, Y_m and Z_m represents the axes of mice $m = 1$ and $m = 2$. In short, an axis or a coordinate that has alphabet G as subscript is with respect to global coordinate system. Take note that the axes of both the mice are parallel and separated by distance D. Mouse $m = 1$ refers to the one locates at the center of the MWR. In other words, coordinate of mouse $m = 1$ with respect to global coordinate system, $\left(x^k_{G,1}, y^k_{G,1}\right)$ is exactly the coordinate of the MWR with respect to global coordinate system, $\left(x^k_{G,\mathrm{MWR}}, y^k_{G,\mathrm{MWR}}\right)$. Equation (1) to (7) are recursive formula derived to compute position, $\left(x^k_{G,\mathrm{MWR}}, y^k_{G,\mathrm{MWR}}\right)$ and orientation, $\alpha^k_{G,\mathrm{MWR}}$ of our MWR.

$$h^k_m = \sqrt{\left(x^k_m\right)^2 + \left(y^k_m\right)^2} \tag{1}$$

$$\alpha^k_m = \tan^{-1}\left(\frac{y^k_m}{x^k_m}\right), \quad x^k_m > 0 \tag{2}$$

$$\begin{bmatrix} x^k_{G,m} \\ y^k_{G,m} \end{bmatrix} = \begin{bmatrix} x^{k-1}_{G,m} \pm h^k_m \cos\left(\alpha^k_m - \alpha^{k-1}_{G,\mathrm{MWR}}\right) \\ y^{k-1}_{G,m} \pm h^k_m \cos\left(\alpha^k_m - \alpha^{k-1}_{G,\mathrm{MWR}}\right) \end{bmatrix} \tag{3}$$

$$\begin{bmatrix} x^k_{G,\mathrm{MWR}} \\ y^k_{G,\mathrm{MWR}} \end{bmatrix} = \begin{bmatrix} x^k_{G,1} \\ y^k_{G,1} \end{bmatrix} \tag{4}$$

$$x^k_{G,\mathrm{diff}} = x^k_{G,2} - x^k_{G,1} \tag{5}$$

$$y^k_{G,\mathrm{diff}} = y^k_{G,2} - y^k_{G,1} \tag{6}$$

$$\alpha^k_{G,\mathrm{MWR}} = \begin{cases} 90° - \tan^{-1}\left(\dfrac{y^k_{G,\mathrm{diff}}}{x^k_{G,\mathrm{diff}}}\right), & x^k_{G,\mathrm{diff}} > 0 \\ -90° - \tan^{-1}\left(\dfrac{y^k_{G,\mathrm{diff}}}{x^k_{G,\mathrm{diff}}}\right), & x^k_{G,\mathrm{diff}} < 0 \\ 0°, & x^k_{G,\mathrm{diff}} = 0 \text{ and } y^k_{G,\mathrm{diff}} > 0 \\ -180°, & x^k_{G,\mathrm{diff}} = 0 \text{ and } y^k_{G,\mathrm{diff}} < 0 \end{cases} \tag{7}$$

where superscript k denotes time step in the recursive calculation. For the '±' sign in Equation (3), '+' is used when $x^k_1 > 0$ whereas '−' is used when $x^k_1 < 0$. Else, if $x^k_1 = 0$, $x^k_{G,m}$ is equal to $x^{k-1}_{G,m}$ and $y^k_{G,m}$ is equal to $\left(x^{k-1}_{G,m} + y^k_m\right)$. Also, from Figure 2, we can notify that $\left(x^k_1 + D\right)$ is always equal to x^k_2.

The proposed dead-reckoned positioning method is sufficiently resistant to wheel slippage and variation of floor characteristic. Sensor fusion of dead-reckoned and absolute positioning sensors can be implemented to further improve the localization by counteracting accumulation of systematic error. Nevertheless, in this paper, the coordinate of the center of our MWR is vitally required to be determinable and as accurate as possible. This is because, the proposed linear angle-to-gain (LA-G) method relies on the coordinate to perform path tracking, which will be explained in Section IV.

III. LINEARIZATION

A linear time-invariant (LTI) system is always simpler to work with, as this type of system is easier to be analyzed and controlled through classical control method and the system output is predictable. However, almost all real-life system exists as non-LTI. K. Ogata mentioned that spacecraft is not a time-invariant system because as time passes, fuel is burned off and the mass of the spacecraft changes [31]. Analogically, the MWR is a not time-invariant system as well because as time passes, power supply from battery depletes and driving torque of the robot's actuator changes. To avoid such happening, two sealed lead acid (SLA) batteries with each rated at 12 V and 2.3 Ah, are connected in parallel and are within 12.2±2 V for the MWR in this paper. The parallel connection ensures sufficient current supply and prolongs operating time. To save time while charging the batteries, an alternating current (AC) to direct current (DC) power switching supply with 12 V and 5 A of output is occasionally used.

Every MWR is unique in its own way; dynamical modeling of non-linearity or uncertainty in the literatures may not be directly applicable for our MWR. Therefore, understanding the unique nominal characteristic of our MWR is an important stepping-stone before path tracking control. The actuators in this paper consist of four Cytron brushed DC geared motors rated at 12 V, 19 RPM and 1 A, and are driven by Cytron four channel motor driver

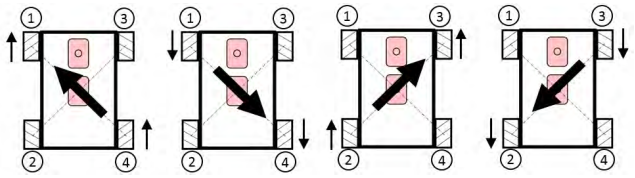

FIGURE 3. Basic actuations to attain maneuvering.

with 8-bit pulse-width modulation (PWM) as input signal. The non-linearity of the actuators can be easily determined from open-loop step responses at different PWM input. Basically, an MWR has four elementary actuations – wheel-1-wheel-4 forward rotation (W1W4_F), wheel-1-wheel-4 backward rotation (W1W4_B), wheel-2-wheel-3 forward rotation (W2W3_F) and wheel-2-wheel-3 backward rotation (W2W3_B), as shown in Figure 3. The control of these basic actuations produces maneuvering motion.

Although the forward and backward actuations (W1W4_F and W1W4_B or W2W3_F and W2W3_B) use the same motors, but forward and backward step inputs may produce slightly different output responses. This may be due to uncertainty such as unaligned center of gravity and center of MWR, uneven mass distribution, irregular wheel-floor friction, tolerance of actuator and other possible factors. To understand the characteristic of our MWR, experimental step responses of all the basic actuations are obtained and as shown in Figure 4.

The non-linear characteristic can first be identified by comparing the gaps (difference) between the final displacements at consecutive PWM values, which are barely inconsistent especially at higher PWM value. Take note that at PWM value of 55, W2W3 produces no output response, whereas W1W4 is opposite. Also, notice that the final displacements of W2W3_F and W2W3_B at each PWM value are different, even though they are actuated by similar motors. To display the non-linearity in a more readable way, all these displacements are converted into velocities and are displayed in Figure 5. Beforehand, since the dead time at different PWM value is slightly different, also, the motion by W1W4 and W2W3 are not perfectly angled at 45°, a formula shown in Equation (8) is used to compute 45°-angled velocity. The negative effect of lengthy dead time is expected to be significant at the moment when the actuator is initiated from static, or during changing of wheel rotating direction. Such time delay (dead time) is one of the factors that causes MWR to deviate in orientation, and is considered as one of the uncertainties. Therefore, it is important to choose an actuator or actuator driver with small dead time, else extra efforts in counteracting the delay is needed. 45°-angled velocity, v_i is given by the following formula:

$$v_i = \frac{\sqrt{\left(y_{f,i}\right)^2 + \left(x_{f,i}\right)^2}}{t_{f,i} - t_{s,i}} \cos\left(45° - \tan^{-1}\left|\frac{y_{f,i}}{x_{f,i}}\right|\right) \tag{8}$$

where i represents the elementary actuation which is either W1W4_F, W1W4_B, W2W3_F or W2W3_B. Notation t_s

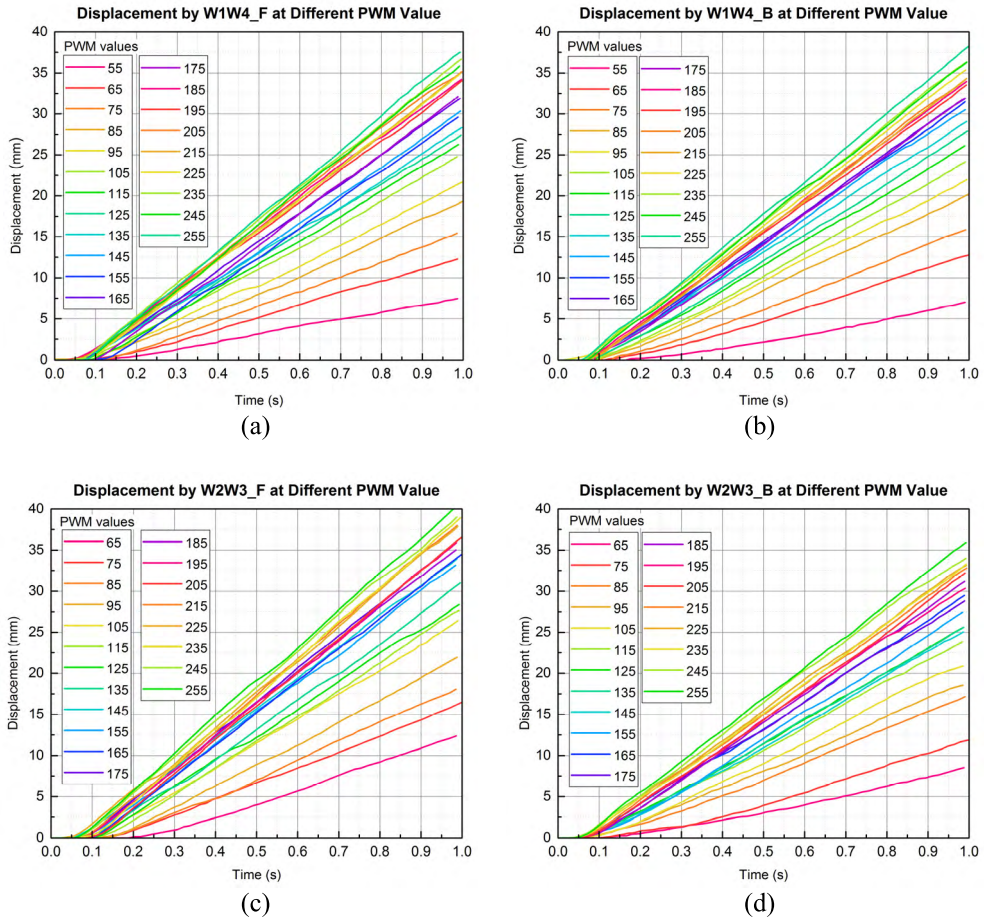

FIGURE 4. Experimental open-loop step responses in term of displacement. (a) Response of wheel-1-wheel-4 in forward rotation (W1W4_F). (b) Response of wheel-1-wheel-4 in backward rotation (W1W4_B). (c) Response of wheel-2-wheel-3 in forward rotation (W2W3_F). (d) Response of wheel-2-wheel-3 in backward rotation (W2W3_B).

denotes the time when the rising in output response starts, whereas t_f, x_f and y_f are final time, final horizontal displacement and final vertical displacement, respectively.

The curve plots shown in Figure 5 clearly present the non-linearity of the actuators, in which similar PWM value but different output velocity. We now understand that each basic actuation has respective characteristic and therefore, our MWR is not suitable to be controlled through PWM. Instead, we inversely control the actuators; control via velocity. Figure 6 shows simplified block diagrams of before (PWM controlled) and after (velocity controlled) linearization. The new block appears between 'Path Tracking Controller' block and 'Motor' block is known as linearization element, which converts velocity to PWM. Each linearization element is based on the nominal characteristic of each actuation.

To determine the linearization elements, firstly, the axes of PWM value versus velocity graphs shown in Figure 5 are swapped, and outcome is as shown in Figure 7. Since the non-linearities perceive an incremental pattern, therefore, instead of creating a lookup table, generating non-linear polynomial equations is feasible and easier. In this case, cubic (third order) polynomial regression is used to generate polynomial equations for W1W4_F, W1W4_B, W2W3_F and W2W3_B as shown in Equations (9–12). By referring Figure 7, take note that the regressions do not include all the PWM values that produce no output response. In order to correspond with the characteristic of the actuators, in our case, first PWM value for W1W4 and W2W3 is 45 and 55, respectively.

$$PWM_{\mathrm{W1W4\_F}} = 0.0056\left(v_{\mathrm{W1W4\_F}}\right)^3 - 0.1603\left(v_{\mathrm{W1W4\_F}}\right)^2 + 2.8629 v_{\mathrm{W1W4\_F}} + 43.4929 \quad (9)$$

$$PWM_{\mathrm{W1W4\_B}} = 0.0077\left(v_{\mathrm{W1W4\_B}}\right)^3 - 0.2702\left(v_{\mathrm{W1W4\_B}}\right)^2 + 4.0447 v_{\mathrm{W1W4\_B}} + 43.4521 \quad (10)$$

$$PWM_{\mathrm{W2W3\_F}} = 0.0061\left(v_{\mathrm{W2W3\_F}}\right)^3 - 0.2335\left(v_{\mathrm{W2W3\_F}}\right)^2 + 3.4245 v_{\mathrm{W2W3\_F}} + 53.9554 \quad (11)$$

$$PWM_{\mathrm{W2W3\_B}} = 0.0055\left(v_{\mathrm{W2W3\_B}}\right)^3 - 0.1041\left(v_{\mathrm{W2W3\_B}}\right)^2 + 1.7440\, v_{\mathrm{W2W3\_B}} + 54.96069 \quad (12)$$

Based on Figure 6, the smallest maximum 45°-angled velocity among the actuations is from W2W3_B, which is valued at around 37.5 mm/s. Therefore, the range of allowable velocity of our MWR is up to 37 mm/s. Take note that when

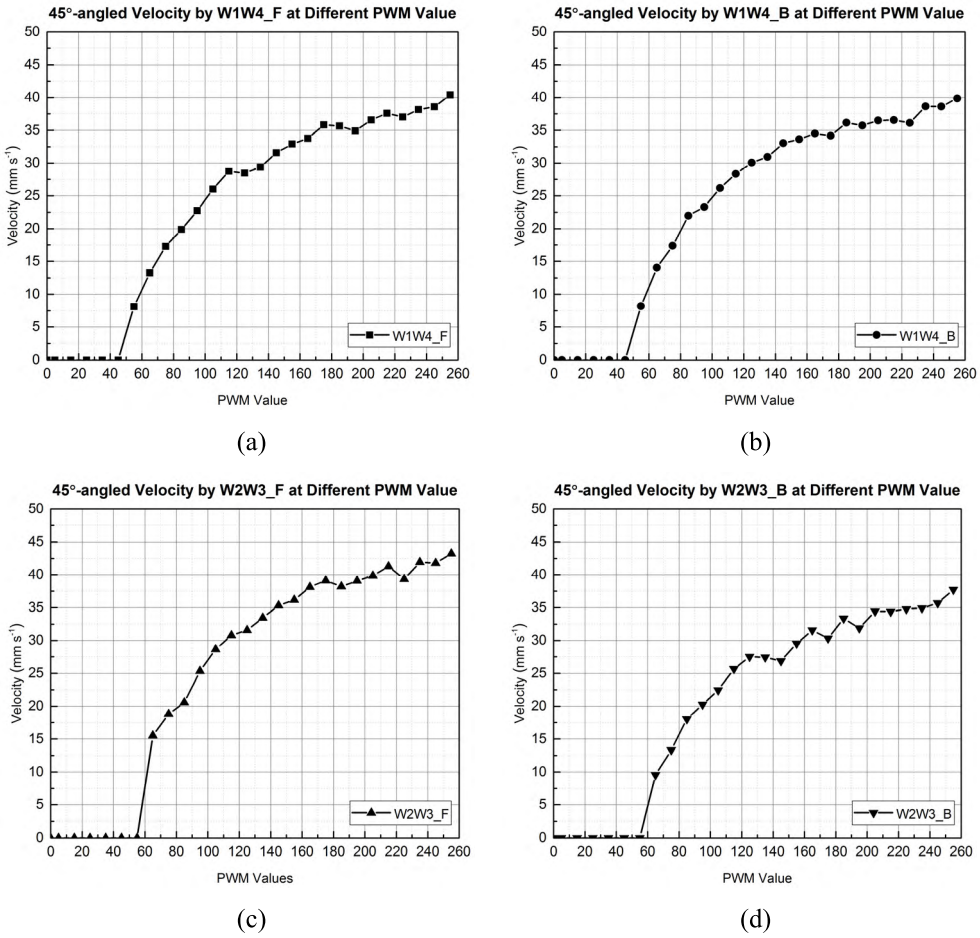

FIGURE 5. Experimental open-loop step responses in term of velocity. (a) Response of wheel-1-wheel-4 in forward rotation (W1W4_F). (b) Response of wheel-1-wheel-4 in backward rotation (W1W4_B). (c) Response of wheel-2-wheel-3 in forward rotation (W2W3_F). (d) Response of wheel-2-wheel-3 in backward rotation (W2W3_B).

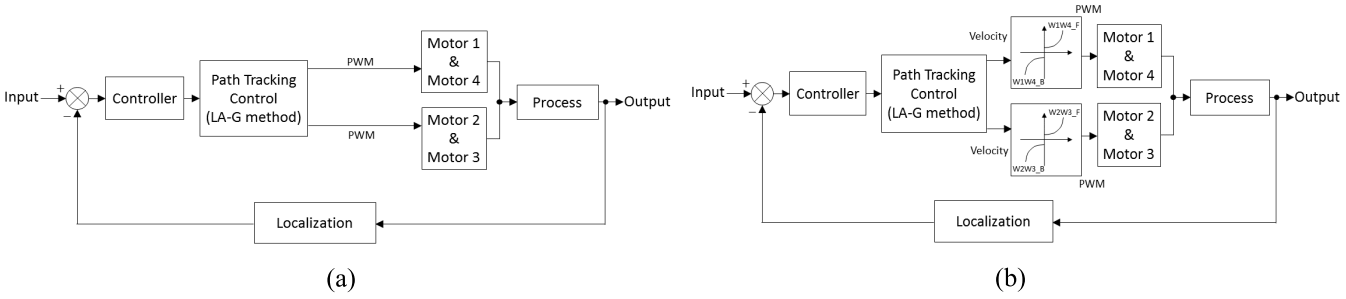

FIGURE 6. Simplified system block diagram: (a) without linearization. (b) with linearization.

velocity is at 0 mm/s, the equations still produce a PWM value due to the offset (Y-axis intercept) presents in the equation. Therefore, in programming, the PWM value at 0 mm/s should be turned off to avoid unnecessary energy wastage. The offsets can be fine-tuned through experimental trial and error so that smaller velocity can be produced accurately. Anyway, due to hardware limitation, it is usually barely able for a brushed DC geared motor to produce and sustain a low velocity or a velocity that is closed to 0 mm/s; the starting velocity or threshold for brushed DC geared motor is usually higher and is fluctuating.

There are plenty of different linearization methods available in literatures, which are suitably applicable for MWR as well. But the linearization method used in this paper is direct and simpler, that is by just using open-loop step responses and polynomial regression. Most importantly, the method is effective because it determines and comprehends the unique characteristic of respective system.

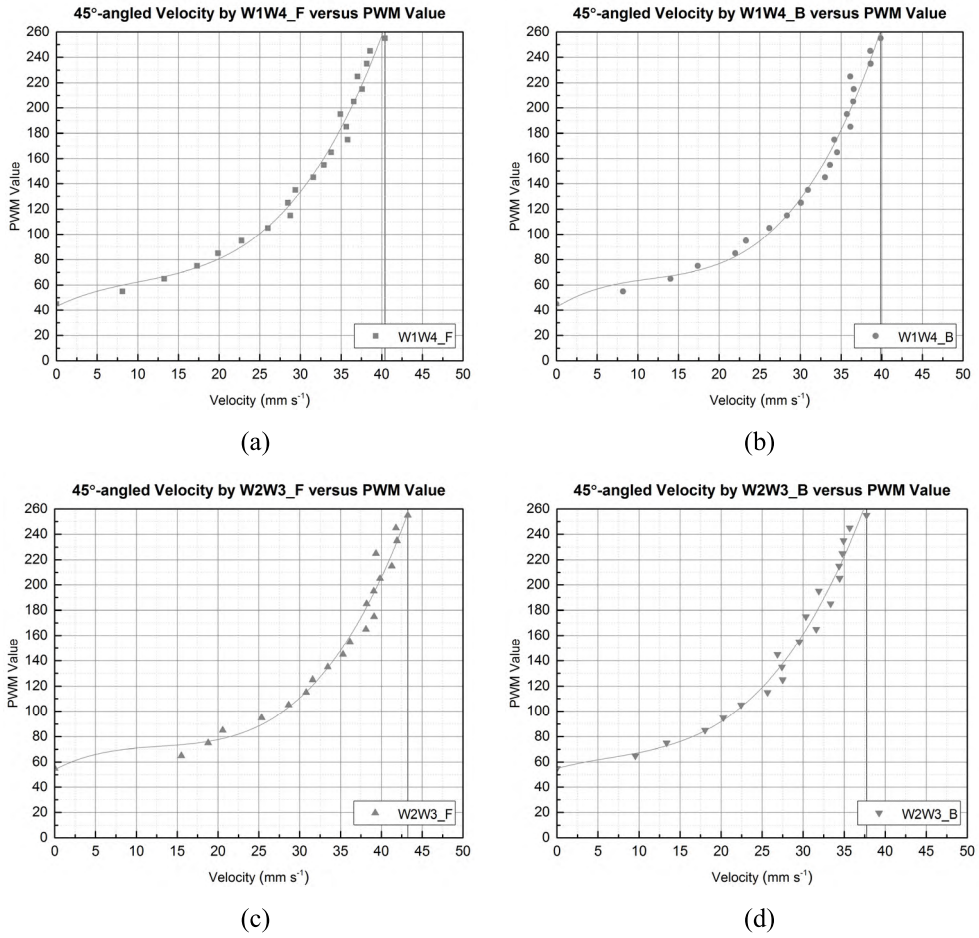

FIGURE 7. Velocity versus PWM value and with curve fitting for: (a) wheel-1-wheel-4 in forward rotation (W1W4_F). (b) wheel-1-wheel-4 in backward rotation (W1W4_B). (c) wheel-2-wheel-3 in forward rotation (W2W3_F). (d) wheel-2-wheel-3 in backward rotation (W2W3_B).

IV. PATH TRACKING CONTROL VIA LINEAR ANGLE-TO-GAIN (LA-G) METHOD

A. CONCEPT AND DESIGN

As what the name of the method implies, LA-G method linearly maps angle to gains which control Mecanum wheels in pairs. The angle that is being mapped is the summation of the MWR's immediate heading angle, and angle between the MWR's immediate position and desired position. As result, the MWR can be controlled to track any angled path. Since the method works in linear, the performance of the path tracking control method is highly dependent on the reliability of the linearization method used. However, it is possible as well to develop a non-linear angle-to-gain of mapping to match the natural non-linearity of the system, but the authors find it simpler to work with a linearized MWR system.

Unlike conventional control method which involves inverse kinematics equation and requires the information of parameters, such as wheel radius, horizontal and vertical distances between center of MWR and center of wheel, the LA-G method requires only center coordinate and heading of MWR as inputs. Moreover, the derivation of inverse kinematics control assumes that the radius of Mecanum wheel is constant [27], no energy loss (no slippage) [25], [32] and perfect instantaneous rotation about robot's center [26]. However, real-life situation completely defies these assumptions. In addition, inverse kinematic control is a velocity-controlled approach and therefore, efforts of unit conversion and nested closed-loop (outer closed-loop controls positioning while inner closed-loop controls angular velocities of the wheels) are often necessary. For LA-G method, it is not affected by the physical parameters and the uncertainties as long as the accuracies of the robot's center coordinate and heading angle are reliable. Also, LA-G method is a displacement-controlled approach as it directly controls the distance between center coordinate of MWR and coordinate of desired position. Overall, LA-G method provides a simpler and instinctive control for MWR in path tracking. Figure 8 is presented below to explain the concept and intuitiveness of LA-G method.

As mentioned in previous section, 45° diagonal motions – W1W4_F, W1W4_B, W2W3_F and W2W3_B are the basic actuations of any MWR. Therefore, by controlling the

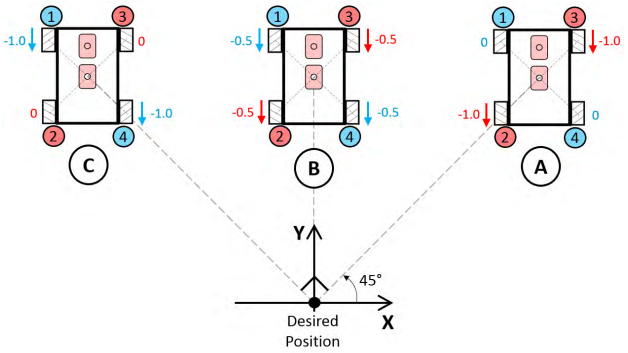

FIGURE 8. Basic of linear angle-to-gain (LA-G) method. Positions A, B and C represent three different starting positions. The decimal values are gains for the Mecanum wheels.

magnitude of these basic actuations, the MWR can maneuver on paths that are beyond 45°-angled. In Figure 8, by comparing Position Ⓐ and Position Ⓒ within the right angle (90°), gain for W1W4 is nil (0) in position Ⓐ, and full magnitude in position Ⓒ. Whereas, W2W3 is vice versa. Therefore, we label full magnitude as gain of 1.0 and negative sign indicates backward direction of wheel rotation. Since position Ⓑ lies at middle, thus the gains are labeled as −0.5. Also, instead of using 0, 0.5 and 1.0, the range of the gain can be altered or amplified to e.g. 0, 1.0 and 2.0, respectively based on desired sensitivity or control system design. The formula that linearly maps the angle to the gain is shown as Equation (13).

$$g_j^k = \left(\theta^k - \theta_{\text{LB}}\right) \times \left(\frac{g_{\text{UB}} - g_{\text{LB}}}{\theta_{\text{UB}} - \theta_{\text{LB}}}\right) + g_{\text{LB}} \qquad (13)$$

where g_j^k, $j = 1, 2, 3$ or 4, is the gain of j^{th} Mecanum wheel and as previous, k is referred as time step. Notations θ_{LB} and θ_{UB} are limits (boundaries) of angle θ^k(input) whereas g_{LB} and g_{UB} are limits of desired gains g_j^k (output). Notations LB and UB denotes lower boundary and upper boundary, respectively. The illustrated LA-G method shown in Figure 8 is partial and introductory, therefore, Figure 9 is prepared to extend the explanation to a complete 360° of coverage. Four sections (quadrants) are founded – (I), (II), (III) and (IV), and are distinguished with different colors for easier understanding and explanation.

Respective values of g_{LB} and g_{UB} can be determined at the boundaries of each quadrant and are ranges from −1.0 to 1.0. From θ_{LB} to θ_{UB} consist of ninety steps of 1°; a total of 90°. For e.g., in Quadrant (I), since $45° \leq \theta^k < 135°$, thus $\theta_{\text{LB}} = 45°$ and $\theta_{\text{UB}} = 134.9°$, and since $0 \geq g_{1\text{or}\,4}^k > -1.00$, thus $g_{\text{LB}} = 0$ and $g_{\text{UB}} = -0.99$. In Figure 9, take note that the gain with negative sign signifies opposite direction of wheel rotation. To intuitively clarify the selection of the boundaries' values, the linear mapping process for W1W4 in Quadrant (I) is illustratively presented in Figure 10. Similar idea is applied for Quadrant (II) and Quadrant (III). However, Quadrant (IV) exhibits a slight difference compared to others, due to the quadrant has angles from 315° to less than 360°

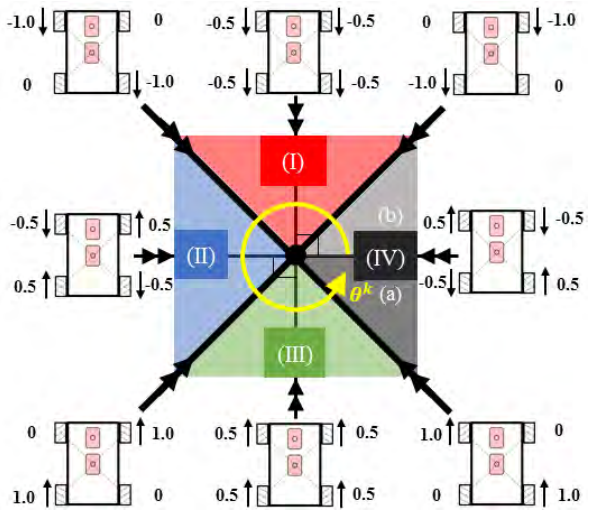

FIGURE 9. Complete illustration of LA-G method. The circle filled with black color at the middle of the illustration represents targeted or desired position.

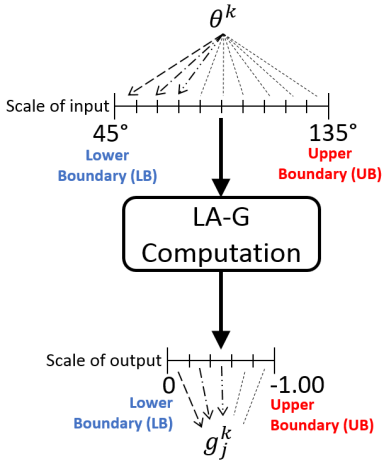

FIGURE 10. Visual representation of LA-G mapping process for W1W4 in Quadrant (I). 45° will be mapped to 0 and so forth. The negative sign in gain merely represents direction of the wheel rotation.

and from 0° to less than 45°. Therefore, Quadrant (IV) is divided into sub-quadrant (a) and sub-quadrant (b); $-315° \leq \theta^k < 360°$ and $0° \leq \theta^k < 45°$, respectively. By using Equation (13) and Figure 9 as reference, gains at different position and angle are computed as Equation (14) and Equation (15), shown at the bottom of the next page.

Figure 9 assumes the heading of the MWR, $\alpha_{G,\text{MWR}}^k$ is 0°. However, it is important to mention that in real-life situation, the heading of MWR will deviate or changed during maneuvering motion due to the uncertainties mentioned earlier. Such changing in heading, which is also the immediate heading of the MWR, $\alpha_{G,\text{MWR}}^k$, is required to be offset. Therefore,

$$\theta^k = \alpha^k + \alpha_{G,\text{MWR}}^k, \qquad (16)$$

where α^k is denoted as the angle between desired position and MWR's immediate position. Notation θ^k is therefore a sum of angle α^k and angle $\alpha_{G,\text{MWR}}^k$ that will be linearly mapped to gains. If there is no heading deviation during path tracking

or maneuvering motion, θ^k is then equals to α^k. Also, in this paper, the method in measuring the MWR's heading angle is as shown in Figure 11. In short, $-180° \leq \alpha^k_{G,\mathrm{MWR}} < 180°$.

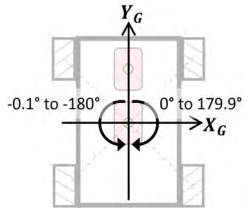

FIGURE 11. Measuring method of MWR's heading angle, $\alpha^k_{G,\mathrm{MWR}}$.

B. ILLUSTRATIVE EXAMPLE

To clearly deliver the idea behind LA-G method and its role in path tracking control, an example of situation which contains three consecutive time steps is presented as shown in Figure 12.

Based on Figure 12, at $k = 0$, $\left(x^0_{G,\mathrm{MWR}}, y^0_{G,\mathrm{MWR}}\right)$ is equal to (0, 0) and $\alpha^0_{G,\mathrm{MWR}}$ is equal to 0°. By using trigonometry rules and coordinates of the MWR's position and desired position, α^0 is calculated as 45°. Therefore, by using Equation (16), $\theta^0 = 45°$ and is located in Quadrant (I). Then, gains for each wheel can be computed by using Equation (14) and Equation (15), as follow:

$$\begin{aligned} g^0_1 &= \left(\theta^0 - 45°\right) \times \frac{(-0.99) - 0}{134.9° - 45°} + 0 = 0 \\ g^0_2 &= \left(\theta^0 - 45°\right) \times \frac{-0.01 - (-1.00)}{134.9° - 45°} + (-1.00) = -1.00 \\ g^0_3 &= g^0_2 = -1.00 \\ g^0_4 &= g^0_1 = 0 \end{aligned} \tag{17}$$

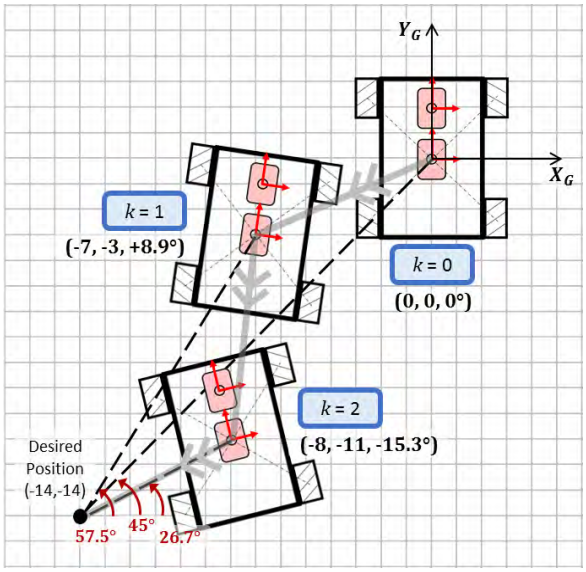

FIGURE 12. Example of maneuvering motion by an MWR in three consecutive time steps displayed on 23 units × 22 units of Cartesian plane. Take note that the global coordinate axes or frame locate(s) at the position where the MWR begins ($k = 0$).

The distance between the instantaneous position (0, 0) and desired position (−14 units, −14 units) is computed as 19.8 units. This value is error signal, ${}^{\mathrm{Pos}}e\,(k)$ for positioning controller. Let a proportional (p) controller,

$${}^{\mathrm{Pos}}CO\,(k) = {}^{\mathrm{Pos}}K_p \times {}^{\mathrm{Pos}}e\,(k) \tag{18}$$

is implemented for the positioning (Pos) control. Notation ${}^{\mathrm{Pos}}CO\,(k)$ denotes the controller's output and ${}^{\mathrm{Pos}}K_p$ denotes the controller's gain. Let ${}^{\mathrm{Pos}}K_p$ equals to 2.0 and therefore

$$g^k_1 = g^k_4 = \begin{cases} \left(\theta^k - 45°\right) \times \left(\dfrac{(-0.99) - 0}{134.9° - 45°}\right) + 0, 45° \leq \theta^k < 135° \text{and} 0 \geq g^k_{1\mathrm{or}4} > -1.00 \\ \left(\theta^k - 135°\right) \times \left(\dfrac{-0.01 - (-1.00)}{224.9° - 135°}\right) + (-1.00)\,, 135° \leq \theta^k < 225° \text{and} -1.00 \leq g^k_{1\mathrm{or}4} < 0 \\ \left(\theta^k - 225°\right) \times \left(\dfrac{0.99 - 0}{314.9° - 225°}\right) + 0, 225° \leq \theta^k < 315° \text{and} 0 \leq g^k_{1\mathrm{or}4} < 1.00 \\ \left(\theta^k - 315°\right) \times \left(\dfrac{0.51 - 1.00}{359.9° - 315°}\right) + 1.00, 315° \leq \theta^k < 360° \text{and } 1.00 \geq g^k_{1\mathrm{or}4} > 0.50 \\ \left(\theta^k - 0°\right) \times \left(\dfrac{0.01 - 0.50}{44.9° - 0°}\right) + 0.50, 0° \leq \theta^k < 45° \text{and} 0.50 \geq g^k_{1\mathrm{or}4} > 0 \end{cases} \tag{14}$$

$$g^k_2 = g^k_3 = \begin{cases} \left(\theta^k - 45°\right) \times \left(\dfrac{-0.01 - (-1.00)}{134.9° - 45°}\right) + (-1.00)\,, 45° \leq \theta^k < 135° \text{and} -1.00 \leq g^k_{2\text{ or }3} < 0 \\ \left(\theta^k - 135°\right) \times \left(\dfrac{0.99 - 0}{224.9° - 135°}\right) + 0, 135° \leq \theta^k < 225° \text{and} 0 \leq g^k_{2\text{ or }3} < 1.00 \\ \left(\theta^k - 225°\right) \times \left(\dfrac{0.01 - 1.00}{314.9° - 225°}\right) + 1.00, 225° \leq \theta^k < 315° \text{and} 1.00 \geq g^k_{2\text{ or }3} > 0 \\ \left(\theta^k - 315°\right) \times \left(\dfrac{-0.49 - 0}{359.9° - 315°}\right) + 0, 315° \leq \theta^k < 360° \text{and } 0 \geq g^k_{2\text{ or }3} > -0.50 \\ \left(\theta^k - 0°\right) \times \left(\dfrac{-0.99 - (-0.50)}{44.9° - 0°}\right) + (-0.50)\,, 0° \leq \theta^k < 45° \text{and} -0.50 \geq g^k_{2\text{ or }3} > -1.00 \end{cases} \tag{15}$$

${}^{\text{Pos}}CO\,(0) = 39.6$. The controller's output value controls the distance between the MWR's immediate position and desired position. To ensure the MWR is tracking desired path while reaching desired position, Equation (19) is used.

$$M^k_{\text{input},j} = {}^{\text{Pos}}CO\,(k) \times g^k_j \tag{19}$$

in which $M^k_{\text{input},j}$ is the input signal for motor driver. Then, the input signals for each Mecanum wheel are computed as follow:

$$\begin{aligned} M^0_{\text{input},1} &= 39.6 \times 0 = 0 \\ M^0_{\text{input},2} &= 39.6 \times (-1.0) = -39.6 \\ M^0_{\text{input},3} &= M^0_{\text{input},2} = -39.6 \\ M^0_{\text{input},4} &= M^0_{\text{input},1} = 0. \end{aligned} \tag{20}$$

In our case, these values stand for velocities and also inputs for the linearizer mentioned in previous section. As usual, the negative sign indicates backward wheel rotation.

Assume that under the presence of disturbance, the resultant controlled outputs from $k = 0$ produces a new position and orientation at $k = 1$. Similar calculation steps are repeated. $\left(x^1_{G,\text{MWR}}, y^1_{G,\text{MWR}}\right)$ is now equal to (−7 units, −3 units). However, at $k = 1$, there is a change in robot's heading, and the angle between the instantaneous position and desired position is no longer 45°; $\alpha^1_{G,\text{MWR}}$ is equal to +8.9° and α^1 is calculated as 57.5°. Therefore,

$$\theta^1 = 57.5° + 8.9° = 66.4° \tag{21}$$

$$\begin{aligned} g^1_1 &= \left(\theta^1 - 45°\right) \times \frac{(-0.99) - 0}{134.9° - 45°} + 0 = -0.24 \\ g^1_2 &= \left(\theta^1 - 45°\right) \times \frac{-0.01 - (-1.00)}{134.9° - 45°} \\ &\quad + (-1.00) = -0.76 \\ g^1_3 &= g^1_2 = -0.76 \\ g^1_4 &= g^1_1 = -0.24 \end{aligned} \tag{22}$$

$$\begin{aligned} {}^{\text{Pos}}e\,(1) &= \sqrt{(-7 - (-14))^2 + (-3 - (-14))^2} \\ &= 13.04\text{units} \end{aligned} \tag{23}$$

$${}^{\text{Pos}}CO\,(1) = 2.0 \times 13.04 = 26.08 \tag{24}$$

$$\begin{aligned} M^1_{\text{input},1} &= 26.08 \times (-0.24) = -10.95 \\ M^1_{\text{input},2} &= 26.08 \times (-0.76) = -19.82 \\ M^1_{\text{input},3} &= M^1_{\text{input},2} = -19.82 \\ M^1_{\text{input},4} &= M^1_{\text{input},1} = -10.95 \end{aligned} \tag{25}$$

Lastly, at $k = 2$, given $\left(x^2_{G,\text{MWR}}, y^2_{G,\text{MWR}}\right)$ and $\alpha^2_{G,\text{MWR}}$ of the MWR are equal to (−8 units, −11 units) and −15.3°, respectively, and α^2 is equal to 26.7°. Therefore,

$$\theta^2 = 26.7° + \left(-15.3°\right) = 11.4°. \tag{26}$$

For $k = 2$, θ^2 is located at Quadrant (IV)(b). Hence, the input angle is $0° \leq \theta^k < 45°$. The complete computation for $k = 2$ is as follows:

$$\begin{aligned} g^2_1 &= \left(\theta^2 - 0°\right) \times \frac{0.01 - 0.50}{44.9° - 0°} + 0.50 = 0.38 \\ g^2_2 &= \left(\theta^2 - 0°\right) \times \frac{-0.99 - (-0.50)}{44.9° - 0°} \\ &\quad + (-0.50) = -0.62 \\ g^2_3 &= g^2_2 = -0.62 \\ g^2_4 &= g^2_1 = 0.38 \end{aligned} \tag{27}$$

$$\begin{aligned} {}^{\text{Pos}}e\,(2) &= \sqrt{(-8 - (-14))^2 + (-11 - (-14))^2} \\ &= 6.71\text{units} \end{aligned} \tag{28}$$

$${}^{\text{Pos}}CO\,(2) = 2.0 \times 6.71 = 13.42 \tag{29}$$

$$\begin{aligned} M^2_{\text{input},1} &= 13.42 \times 0.38 = 5.01 \\ M^2_{\text{input},2} &= 13.42 \times (-0.62) = -8.32 \\ M^2_{\text{input},3} &= M^2_{\text{input},2} = -8.32 \\ M^2_{\text{input},4} &= M^2_{\text{input},1} = 5.01 \end{aligned} \tag{30}$$

By comparing Equations (20), (25) and (30), we can notice that the inputs for motor driver (velocity) decreases as the MWR approaches desired position. Also, at different position and heading, LA-G method produces different gains to control the Mecanum wheels. The example shown has only one desired position (step input), however, generating multiple consecutives positions along the desired path (ramp input) is feasible as well and may produce better result.

V. EXPERIMENTAL SETUP AND PERFORMANCE

A. EXPERIMENTAL SETUP

The Mecanum-wheeled robot (MWR) developed in this paper is equipped with four 60 mm diameter of Mecanum wheels.

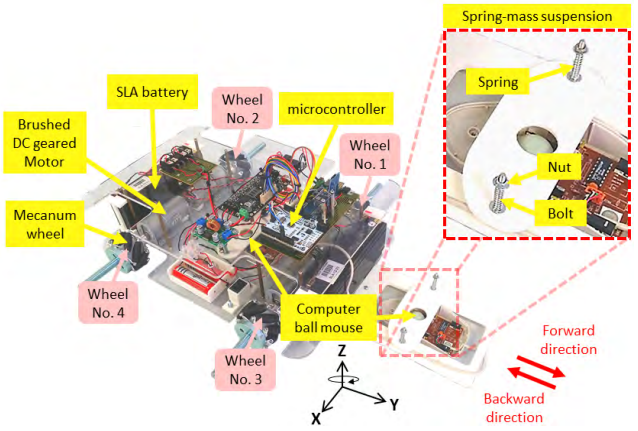

FIGURE 13. Experimental setup of the MWR.

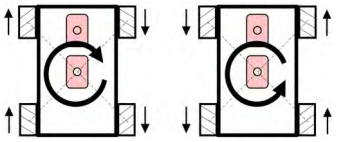

FIGURE 14. Basic actuations for heading control.

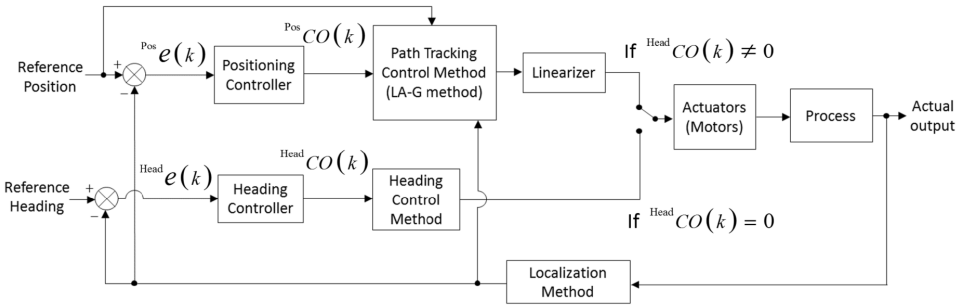

FIGURE 15. Block diagram of the MWR control system.

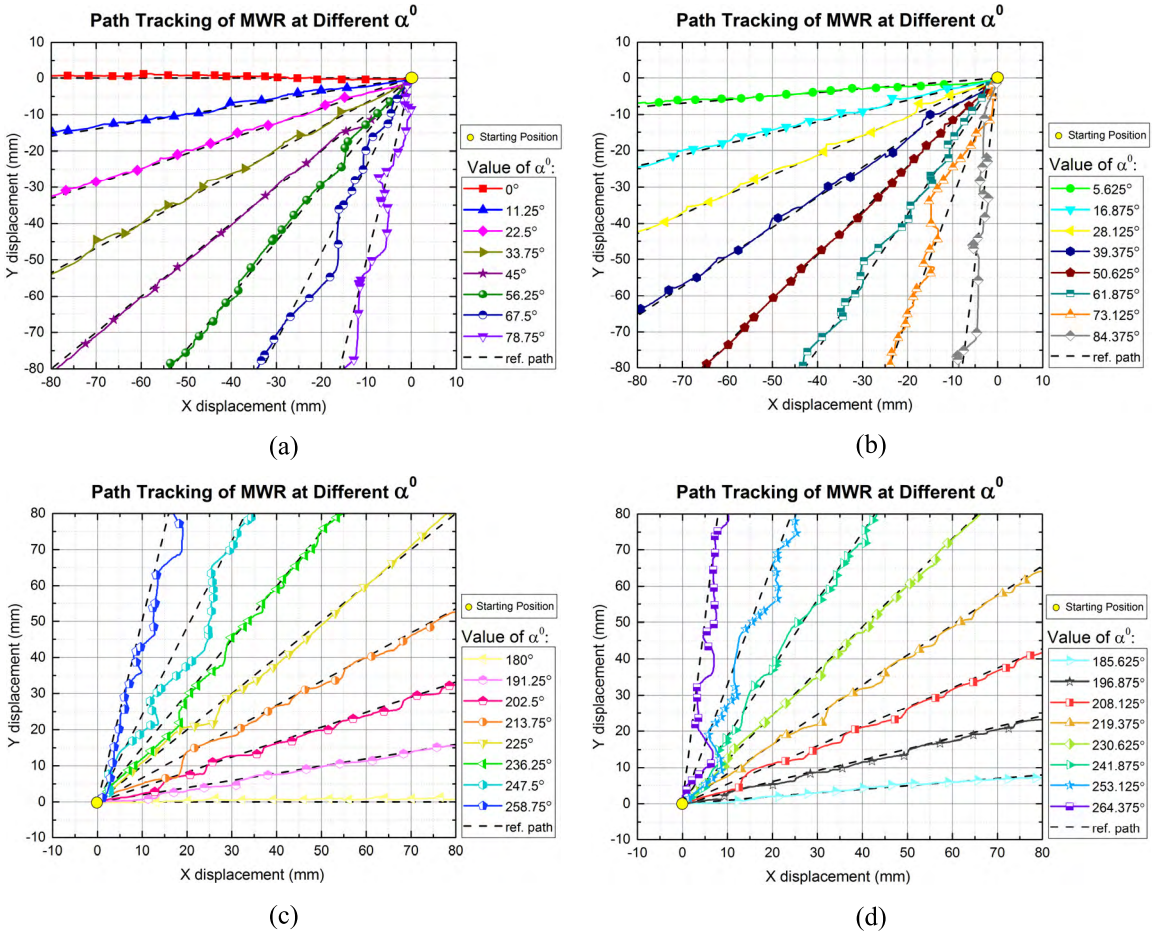

FIGURE 16. Tracking of straight paths with: (a) & (b) reference paths angled from 0° to 84.375°, with step of 5.625°. (c) & (d) reference paths angled from 180° to 264.375°, with step of 5.625°.

The wheels are driven by four Cytron SPG50-180K brushed DC geared motor with each rated at 12 V, 1 A, 19 RPM and 15 kgf·cm, with power source from two parallelly connected 12 VDC SLA batteries. Two A4 Tech computer ball mice with PS/2 protocol are used as localization sensors. The mice are supported by simple spring-mass suspension system to enhance the contact between surface of experimental area and the sensors. Each mouse has sampling time of 5±1 ms and resolution of 10 μm. Cytron 32-bit ARM Cortex-M0 microcontroller with clock speed of 50 MHz is used to read the sensors, process conditions and execute control commands. Overall, the sampling time of the control system is 15±3 ms. Figure 13 shows the experimental setup of the MWR.

The mass of the MWR is considerably small and the friction between the wheel and the surface of experimental area is inadequate. Therefore, when only one Mecanum wheel tries to drive the MWR, the wheel slips. To prevent such inefficiency, the wheels are required to work in pairs.

TABLE 1. IAE, SD and COV of the straight path tracking.

Value of α^0	Integral of Absolute Error, IAE (mm)				Standard Deviation, SD	Coefficient of Variation, COV
	Experiment 1	Experiment 2	Experiment 3	Experiment 4		
0°	40.3042	44.3559	47.6094	44.2468	2.5888	0.0677
5.625°	56.5241	52.7800	55.3524	58.4963	2.0685	0.0428
11.25°	44.4317	43.0395	50.1296	44.7521	2.6999	0.0684
16.875°	44.3827	47.2664	48.1921	48.6182	1.6514	0.0405
22.5°	48.2832	53.0816	39.9841	43.0782	5.0011	0.1253
28.125°	43.0684	40.4215	54.4685	50.0120	5.5584	0.1366
33.75°	48.9995	55.2309	62.0477	57.2255	4.6801	0.0967
39.375°	58.3929	67.2962	66.8693	76.8141	6.5198	0.1118
45°	58.4406	90.6434	76.3466	85.6788	12.2874	0.1824
50.625°	21.0245	32.8749	26.5270	33.9511	5.2104	0.2104
56.25°	67.6804	63.5608	85.1153	94.1579	12.5114	0.1861
61.875°	73.5338	132.6261	81.2383	117.1902	24.5314	0.2801
67.5°	190.3591	189.4723	121.0979	132.4784	31.8207	0.2320
73.125°	145.7482	263.6682	177.3315	268.0824	53.3722	0.2884
78.75°	158.6492	279.7029	180.2006	343.9254	75.1152	0.3605
84.375°	154.9967	267.8824	226.2013	385.6138	123.3795	0.5022
180°	51.7746	55.3447	48.3223	57.6793	3.5518	0.0770
185.625°	23.4338	19.8430	27.9709	25.4348	2.9712	0.1419
191.25°	59.5311	43.4604	58.1263	57.3398	6.4874	0.1372
196.875°	62.9955	74.1529	55.3460	60.5511	6.8683	0.1254
202.5°	77.4131	75.1783	72.3299	90.1796	6.8263	0.1001
208.125°	77.5641	70.6496	81.0745	80.6324	4.1689	0.0621
213.75°	62.0477	57.2254	55.2309	48.9994	4.6801	0.0967
219.375°	72.2528	60.4509	90.3723	87.1848	12.0175	0.1789
225°	100.2419	120.9918	96.5034	136.0430	16.0387	0.1633
230.625°	49.7222	47.1795	63.9637	70.7720	9.8013	0.1954
236.25°	101.7414	95.4620	92.7470	108.1613	5.9571	0.0691
241.875°	122.0085	92.6333	167.2701	122.0085	26.6853	0.2446
247.5°	240.5075	198.1852	290.0354	287.4043	37.7880	0.1718
253.125°	287.9293	328.2989	223.3463	260.1123	38.3982	0.1613
258.75°	251.9132	296.3734	226.6192	384.6335	60.1328	0.2395
264.375°	391.9439	513.1867	445.9184	692.2796	113.2220	0.2559

Basic actuations for path tracking (positioning) control are as shown in Figure 3, whereas basic actuations for heading control are shown in Figure 14.

From both Figure 3 and Figure 14, we can notice that each actuation is executed by two wheels with identical vector. Therefore, in this experiment, path tracking control and heading control are two closed loops. However, closed loop of heading control is given priority. In other words, when output of the heading controller, ${}^{\text{Head}}CO\,(k)$ is not equal to 0, the MWR will be controlled to compensate the heading error only. Once the heading error, ${}^{\text{Head}}e\,(k)$ is compensated and ${}^{\text{Head}}CO\,(k)$ is equal to 0, then closed-loop positioning control is resumed. Figure 15 generally shows the system block diagram of the MWR in this experiment. To exclusively evaluate the effectiveness of the proposed methods without additional scheme or support, simple P controllers are implemented for both the path tracking (positioning) control and heading control with controllers' gains of ${}^{\text{Pos}}K_p = 2.0$ and ${}^{\text{Head}}K_p = 1.0$, respectively. Such setting is constant for all the path tracking experiments in this section.

The experiments involved two types of path tracking, that is, straight paths and complex-shaped paths. The complex-shaped path refers to 8-shaped and ∞-shaped of paths. Whereas, the straight paths refer to linear paths that are angled from $\alpha^0 = 0°$ to $\alpha^0 = 84.375°$ and $\alpha^0 = 180°$ to $\alpha^0 = 264.375°$ with respect to horizontal axis of final position (kindly refer Figure 12 for method of measuring α^0). The straight paths have increment of 5.625° consecutively. 5.625° is one-eighth $\left(1/8\right)$ of 45° and also represents the resolution that our MWR can reach. The reason why $0° \leq \alpha^0 \leq 84.375°$ and $180° \leq \alpha^0 \leq 264.375°$ are involved, but not $0° \leq \alpha^0 < 360°$, is because such design of experiment adequately

TABLE 2. ISE, SD and COV of the straight path tracking.

Value of α^0	Integral of Squared Error, IAE (mm^2)				Standard Deviation, SD	Coefficient of Variation, COV
	Experiment 1	Experiment 2	Experiment 3	Experiment 4		
0°	5.6808	7.3724	7.7154	7.4886	0.9333	0.1321
5.625°	10.0985	8.8783	9.4978	13.7293	2.1767	0.2063
11.25°	7.9496	8.6055	10.4205	8.3325	1.0959	0.1241
16.875°	7.4586	8.8906	8.2802	9.9736	1.0592	0.1224
22.5°	16.5617	12.7163	7.6198	9.3225	3.9533	0.3421
28.125°	8.2517	10.6487	17.1621	10.6529	3.8265	0.3276
33.75°	13.1646	20.4405	24.0612	13.4693	5.3671	0.3018
39.375°	16.2604	32.7011	21.9357	47.9090	13.9222	0.4687
45°	15.4815	37.8384	26.9814	30.6842	9.3362	0.3365
50.625°	1.1469	3.5943	2.1024	2.7563	1.0348	0.4312
56.25°	12.9329	11.4976	20.1479	25.5583	6.5531	0.3737
61.875°	15.5126	62.1118	22.9618	58.0063	23.8229	0.6009
67.5°	172.1097	92.6865	79.8307	88.4629	42.8932	0.3962
73.125°	115.9128	401.7811	134.8935	302.2981	137.2257	0.5748
78.75°	148.5817	386.0415	140.4309	452.2982	160.9019	0.5709
84.375°	167.6014	259.6913	241.0480	322.8912	63.9205	0.2579
180°	7.8509	9.5612	6.4847	8.7396	1.3167	0.1614
185.625°	1.9159	1.6199	2.4737	2.0162	0.3540	0.1765
191.25°	10.7471	7.2144	10.4466	9.7727	1.6064	0.1683
196.875°	13.3183	17.0712	9.7231	13.3347	3.0001	0.2245
202.5°	20.1741	19.1590	20.9417	30.3393	5.1756	0.2285
208.125°	22.2672	20.1016	25.7105	28.9264	3.8791	0.1600
213.75°	74.8675	53.5349	33.4943	69.9610	18.6908	0.3225
219.375°	23.9482	14.7663	41.2061	47.6334	15.1761	0.4759
225°	34.1080	47.5647	30.9459	75.9004	20.4892	0.4347
230.625°	8.7934	6.9691	14.6574	17.1322	4.7939	0.4033
236.25°	51.6853	49.6655	38.4871	58.6889	8.3756	0.1688
241.875°	81.9475	61.8588	121.0863	81.9475	24..7970	0.2860
247.5°	248.1476	212.2391	389.6807	467.3580	119.7147	0.3635
253.125°	531.0519	522.1308	251.3384	355.6087	135.7172	0.3270
258.75°	371.8840	395.1735	220.9060	509.1650	118.5465	0.3167
264.375°	593.7430	669.5846	572.3694	764.7759	87.0792	0.1339

involves the operations all basic actuations – W1W4_F, W1W4_B, W2W3_F and W2W3_B. Thus, optimal experimental validation is realized. Finally, experiments of the straight paths are repeated three times to obtain standard deviation and coefficient of variation (COV) based on integral of absolute error (IAE) and integral of squared error (ISE).

B. TRACKING PERFORMANCE OF STRAIGHT PATH

Figure 16 compiles and shows the performances of the MWR in tracking designated straight paths. Take note that the coordinate of 'Starting Position' is always (0, 0). Generally, the overall result is promising because the MWR is able to track all the given paths. Even though there are deviations along the paths, the result shows that the MWR was responsive towards the error and was successfully controlled to drive back on correct course. However, deviation from reference path (error) can be observed in most of the tracking. Some of the error is observed to had sustain for a short but significant length of motion. As the motion continues, the error grows larger. When the error is large enough, the actuator is finally responsive and the MWR is driven closer to or back on track. Nevertheless, this happening is expected because the controller implemented for the positioning is merely a P controller who has no integral action.

Moreover, from $\alpha^0 = 61.875°$ up to $\alpha^0 = 84.375°$ and from $\alpha^0 = 247.5°$ up to $\alpha^0 = 264.375°$, the tracking performance significantly deteriorates. or in other words, the MWR struggles to track the reference path when the value of α^0 is closes to 90° and 270°, respectively. By referring Figure 9, at α^0 equals to 90° and 270° (or, at θ^0 equals to 90° and 270° because $\alpha^0_{G,\mathrm{MWR}}$ equals to 0°), all of the wheels are rotating in the same direction – backward and forward, respectively. Therefore, for paths like $\alpha^0 = 84.375°$ and $\alpha^0 = 264.375°$, who are closed to 90° and 270° respectively,

small yet distinguishable velocity difference is required. The large fluctuation or deviation in these paths indicates that the actuators (motors) struggle to produce and maintain a relatively small velocity difference.

IAEs, ISEs and their standard deviations (SDs) and COVs of the experimental straight paths trackings are recorded in Table I and Table II, respectively. For the IAEs, all COVs are below 0.50 except $\alpha^0 = 84.375°$, who is recorded with 0.5022 of COV. Whereas for the ISEs, $\alpha^0 = 61.875°$, $\alpha^0 = 73.125°$ and $\alpha^0 = 78.75°$ are recorded with COVs of more than 0.50.

C. TRACKING PERFORMANCE OF COMPLEX-SHAPED PATH

To further evaluate the proposed methods and control system, the MWR is tested with more complicated paths. Figure 17 depicts the trackings of 8-shaped and ∞-shaped paths. Based on the result, the MWR displays successful tracking in these paths; the MWR manages to drive back on course even though deviation occurs. The deviation that happened within −10 mm to −100 mm of x-displacement in Figure 17(b) may be originated from irresponsive W2W3_B actuation. This may be due to non-linearity or dead zone of the actuator. Fine tuning of the linearizer can be carried out to improve the result. Afterall, the values of the error arose during the tracking are not more than 10mm.

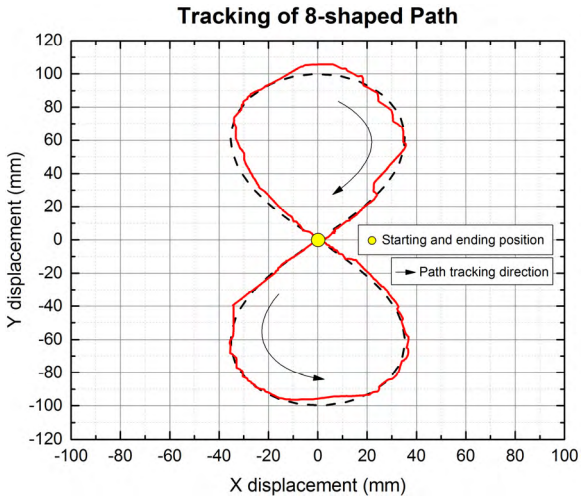

FIGURE 17. Tracking of complex-shaped path: (a) with shape of '8'. (b) with shape of '∞'.

VI. CONCLUSION

In this paper, comprehensive methods in developing and controlling an MWR in tracking various straight paths and complex paths have been presented. This paper starts by realizing a localization method, that is by using computer ball mice as positioning sensor. Such design is simply sufficient to achieve fast and accurate positioning without being affected by wheel slippage. Then, development of linearizers by using open-loop step responses and polynomial regression is carried out for all the basic actuations. Open-loop step response is important and useful in directly determining the unique non-linear characteristic of the MWR system. Next, linear angle-to-gain (LA-G) method is proposed as an intuitive path tracking control method for MWR. As the name of the method implies, the method linearly maps the summation of angle between current and desired position, and heading angle of the MWR, to gains that control Mecanum wheels in pairs. The method is straightforward and simple because it does not require the knowledge of parametric values. In addition, LA-G method is directly a displacement-controlled method and thus require no unit conversion. Finally, by combining all the methods and by using only P controllers, the MWR successfully demonstrate tracking of complex-shaped paths and straight paths that are beyond the common 45°-angled paths. In other words, the MWR manages to track the given paths with a more straightforward approach and a simpler control system. Although the result displays successful tracking performance, but improvement on the control system of the MWR in counteracting steady-state error and actuator's dead zone is desired, which will be done in future work.

ACKNOWLEDGMENT

The authors would like to express their gratitude to Motion Control Research Laboratory, Universiti Teknikal Malaysia Melaka (UTeM) for the provision of facilities and equipment.

REFERENCES

[1] R. Dillmann, J. Kreuziger, and F. Wallner, "PRIAMOS: An experimental platform for reflexive navigation," *Robot. Auton. Syst.*, vol. 11, nos. 3–4, pp. 195–203, 1993.
[2] Z. W. Wu, C. J. Zhang, D. L. Tan, X. B. Li, and Y. C. Wang, "A multirobot coordination system," *IFAC Proc. Volumes*, vol. 27, no. 14, pp. 903–909, 1994.
[3] C. Bühler, R. Hoelper, H. Hoyer, and W. Humann, "Autonomous robot technology for advanced wheelchair and robotic aids for people with disabilities," *Robot. Auton. Syst.*, vol. 14, nos. 2–3, pp. 213–222, 1995.
[4] S. Guo, Q. Diao, and F. Xi, "Vision based navigation for Omni-directional mobile industrial robot," *Procedia Comput. Sci.*, vol. 105, pp. 20–26, Jan. 2017.

[5] C. Kirsch and C. Röhrig, "Global localization and position tracking of an Automated Guided Vehicle," *IFAC Proc. Volumes*, vol. 18, no. 1, pp. 14036–14041, 2011.
[6] T. Asfour *et al.*, "Toward humanoid manipulation in human-centred environments," *Robot. Auton. Syst.*, vol. 56, no. 1, pp. 54–65, 2008.
[7] A. Cheong, M. W. S. Lau, E. Foo, J. Hedley, and J. W. Bo, "Development of a robotic waiter system," *IFAC-PapersOnLine*, vol. 49, no. 21, pp. 681–686, 2016.
[8] M. de Villiers and N. S. Tlale, "Development of a control model for a four wheel Mecanum vehicle," *J. Dyn. Syst., Meas., Control*, vol. 134, no. 1, pp. 1–5, 2012.
[9] L. Ferrière, P. Fisette, B. Raucent, and B. Vaneghem, "Contribution to the modelling of a mobile robot equipped with universal wheels," *IFAC Proc. Volumes*, vol. 30, no. 20, pp. 675–682, 1997.
[10] K. Nagatani, S. Tachibana, M. Sofne, and Y. Tanaka, "Improvement of odometry for omnidirectional vehicle using optical flow information," in *Proc. IEEE/RSJ Int. Conf. Intell. Robots Syst. (IROS)*, vol. 1, Oct./Nov. 2000, pp. 468–473.
[11] T. Peng, J. Qian, B. Zi, J. Liu, and X. Wang, "Mechanical design and control system of an Omni-directional mobile robot for material conveying," *Procedia CIRP*, vol. 56, pp. 412–415, Jan. 2016.
[12] M. Killpack, T. Deyle, C. Anderson, and C. C. Kemp, "Visual odometry and control for an omnidirectional mobile robot with a downward-facing camera," in *Proc. IEEE/RSJ Int. Conf. Intell. Robots Syst.*, Oct. 2010, pp. 139–146.
[13] A. Shimada, S. Yajima, P. Viboonchaicheep, and K. Samura, "Mecanum-wheel vehicle systems based on position corrective control," in *Proc. IEEE 31st Annu. Conf. Ind. Electron. Soc. (IECON)*, Nov. 2005, pp. 2077–2082.
[14] P. Viboonchaicheep, A. Shimada, and Y. Kosaka, "Position rectification control for mecanum wheeled Omni-directional vehicles," in *Proc. IEEE 29th Annu. Conf. Ind. Electron. Soc. (IECON)*, Nov. 2003, pp. 854–859.
[15] B. Chu, "Mobile robot position control algorithm based on multiple ultrasonic distance sensors," in *Proc. ICCAS*, Oct. 2015, pp. 1238–1240.
[16] P. Weckesser and R. Dillmann, "Modeling unknown environments with a mobile robot," *Robot. Auton. Syst.*, vol. 23, no. 4, pp. 293–300, 1998.
[17] E. Uyar and L. Mutlu, "IFAC workshop on advances in control and automation theory for transportation applications guidance and control of an unmanned holonomic robot for transport applications," *IFAC*, vol. 46, no. 25, pp. 188–192, 2013.
[18] S.-J. Huang and Y.-W. Shiao, "2D path control of four Omni wheels mobile platform with compass and gyroscope sensors," *Sens. Actuators A, Phys.*, vol. 234, pp. 302–310, Oct. 2015.
[19] C. Röhrig, D. Heß, C. Kirsch, and F. Künemund, "Localization of an omnidirectional transport robot using IEEE 802.15.4a ranging and laser range finder," in *Proc. IEEE/RSJ Int. Conf. Intell. Robots Syst.*, Oct. 2010, pp. 3798–3803.
[20] C. M. Kumile and N. S. Tlale, "Intelligent distributed fuzzy logic control system (IDFLCS) of a mecanum wheeled autonomous guided vehicle," in *Proc. IEEE Int. Conf. Mechatron. Automat.*, vol. 1, Jul./Aug. 2005, pp. 131–137.
[21] Fahmizal and C.-H. Kuo, "Trajectory and heading tracking of a mecanum wheeled robot using fuzzy logic control," in *Proc. Int. Conf. Instrum., Control Automat. (ICA)*, Aug. 2016, pp. 54–59.
[22] C.-C. Tsai and H.-L. Wu, "Nonsingular terminal sliding control using fuzzy wavelet networks for Mecanum wheeled Omni-directional vehicles," in *Proc. Int. Conf. Fuzzy Syst.*, Jul. 2010, pp. 1–6.
[23] L.-C. Lin and H.-Y. Shih, "Modeling and adaptive control of an Omni-mecanum-wheeled robot," *Intell. Control Autom.*, vol. 4, pp. 166–179, May 2013.
[24] V. Alakshendra and S. S. Chiddarwar, "A robust adaptive control of mecanum wheel mobile robot: Simulation and experimental validation," in *Proc. IEEE/RSJ Int. Conf. Intell. Robots Syst. (IROS)*, Oct. 2016, pp. 5606–5611.
[25] Y. Jia, X. Song, and S. S.-D. Xu, "Modeling and motion analysis of four-mecanum wheel Omni-directional mobile platform," in *Proc. CACS Int. Autom. Control Conf. (CACS)*, Dec. 2013, pp. 328–333.
[26] N. Tlale and M. de Villiers, "Kinematics and dynamics modelling of a mecanum wheeled mobile platform," in *Proc. 15th Int. Conf. Mechatron. Mach. Vis. Pract. (M2VIP)*, no. 3, Dec. 2008, pp. 657–662.
[27] S. L. Dickerson and B. D. Lapin, "Control of an Omni-directional robotic vehicle with Mecanum wheels," in *Proc. Nat. Telesyst. Conf. (NTC)*, 1991, vol. 810, nos. 1–2, pp. 323–328.
[28] J. A. Cooney, W. L. Xu, and G. Bright, "Visual dead-reckoning for motion control of a Mecanum-wheeled mobile robot," *Mechatronics*, vol. 14, pp. 623–637, Jul. 2004.
[29] A. Bonarini, M. Matteucci, and M. Restelli, "Automatic error detection and reduction for an odometric sensor based on two optical mice," in *Proc. IEEE Int. Conf. Robot. Autom.*, Apr. 2005, pp. 1675–1680.
[30] D. Sekimori and F. Miyazaki, "Precise dead-reckoning for mobile robots using multiple optical mouse sensors," in *Informatics in Control, Automation and Robotics II*. Dordrecht, The Netherlands: Springer, 2007, pp. 145–151.
[31] K. Ogata, *Modern Control Engineering*, 5th ed. Upper Saddle River, NJ, USA: Prentice-Hall, 2010.
[32] P. Kiddee and A. Shimada, "A controller design on person following Omni-directional vehicle robots," in *Proc. SICE Annu. Conf.*, Sep. 2007, pp. 1043–1047.

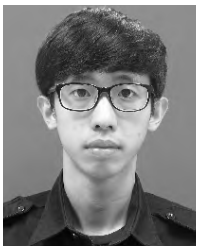

JOE SIANG KEEK was born in Selangor, Malaysia, in 1993. He received the B.Eng. degree (Hons.) in mechatronics engineering from Universiti Teknikal Malaysia Melaka, Malaysia, in 2017, where he is currently pursuing the M.Sc. degree in electrical engineering and also conducts his researches and studies with the Motion Control Research Laboratory, Faculty of Electrical Engineering. His research interest includes motion control and control system design of autonomous robots.

SER LEE LOH was born in Johor, Malaysia, in 1983. She received the B.S. degree in industrial mathematics, and the M.S. and Ph.D. degrees in mathematics from Universiti Teknologi Malaysia, Malaysia, in 2006, 2006, and 2011, respectively. From 2012 to 2014, she was a Lecturer with Sunway University, Malaysia. Since 2014, she has been a Senior Lecturer with the Department of Power Industrial Engineering, Universiti Teknikal Malaysia Melaka, Malaysia, where she has been with the Department of Mechatronics Engineering, since 2019. Her research interests include combinatorial optimization, single-row routing, artificial intelligence, mathematical modeling, and optimization.

SHIN HORNG CHONG received the B.Eng. and M.Sc. degrees in electrical engineering from Universiti Teknologi Malaysia, Malaysia, in 2001 and 2003, respectively, and the Dr. Eng. degree in mechano-micro engineering from the Tokyo Institute of Technology (Tokyo Tech), Japan, in 2010. She is currently an Associate Professor with the Department of Control, Instrumentation and Automation, Faculty of Electrical Engineering, Universiti Teknikal Malaysia Melaka. Her research interests include motion control, mechatronic systems design and modeling, precision engineering, and rehabilitation systems.